Excitation of stripe domain patterns by propagating acoustic waves in an oriented nematic film*

K. Miyano† and Y. R. Shen*
Physics Department, University of California, Berkeley, California 94720
and Materials and Molecular Research Division, Lawrence Berkeley Laboratory, Berkeley, California 94720
(Received 14 June 1976)

Stripe domain patterns have been observed in a nematic liquid crystal film excited by ultrasonic waves propagating in a sandwiched glass-nematic-glass medium. The effect was found to be due to molecular reorientation induced by acoustic streaming in the nematic film. Based on a simple fluid dynamical model, we calculated the propagating acoustic modes, their nonlinear mixing which causes acoustic streaming, and the resultant shear flow reorientation of the director which produces the birefringent stripe patterns. Our calculations show quantitative agreement with the measured acoustic modes and the observed stripe domain patterns.

I. INTRODUCTION

It has been shown that acoustic waves can influence the optical properties of nematic crystals.[1-6] A qualitative discussion on the subject has been given by Helfrich.[1] Because of anisotropy in the viscoelasticity and sound attenuation, a uniform longitudinal sound wave can produce a steady transverse force, which in turn gives rise to a transverse mass flow and reorientation of molecules. In the case of a thin homeotropic nematic film (i.e., the director of molecular alignment being normal to the film surface) with sound waves propagating along the normal of the film, the molecular orientation becomes unstable and undergoes a transition at a critical acoustic power similar to the well-known Fredericksz transition.[7] Many such experiments have been reported[2] but quantitative analysis, especially of its steady-state configuration after the transition, is still not available.

Another geometry has also been used where shear vibration in fluid perpendicular to the director is important. The experiments employed propagating surface waves[3] or longitudinal bulk waves[4] along the substrate. Existing calculations[4,5] in this case assumed that the observed results came from the molecular reorientation in the boundary layers induced by the viscoelastic shear motion of the sound, which is first order in the sound amplitude. However, they were not successful in explaining the experimental results.

We have recently studied the propagation of ultrasonic waves in homeotropic nematic films sandwiched between glass plates. With the sandwiched film between crossed polarizers, we observed a semiperiodic stripe pattern.[3,6] We found that flow reorientation of molecules in the nematic film was responsible for the observed pattern, while acoustic streaming resulting from nonlinear mixing of the propagating acoustic modes in the film was the cause of the fluid flow. A preliminary analysis of the experimental results has already been reported.[6] In this paper we would like to give a full account of the calculation and the experiment.

In Sec. II, we show the detailed calculation for flow reorientation induced by ultrasonic wave propagation in a homeotropic nematic film. In Sec. III, we describe the experimental technique. Finally, in Sec. IV, we present the experimental results, comparison between theory and experiment, and discussion.

II. THEORY

In this section, we first give a theoretical description of acoustic-wave propagation in a fluid film sandwiched between two identical solid planes. We then calculate the acoustic streaming of the fluid induced by the propagating acoustic waves. In a nematic liquid-crystal film, the streaming causes flow reorientation of molecules and hence tilts the optic axis of the anisotropic film. We finally evaluate the optical-transmission coefficient of the film between crossed polaroids in order to compare the calculation with the experimental results.

Because a rigorous treatment of the hydrodynamical problem is extremely difficult, a number of simplifying assumptions are made in our calculation. It may be helpful to first discuss these assumptions here before we go into the details. Based on the observation of almost identical acoustic streaming patterns in a water film to those in a nematic film, as will be described at the end of Sec. IV, we believe that the anisotropy of the nematics is only of secondary importance to the acoustic streaming. In fact, the structure of acoustic streaming (e.g., periodicity of the pattern)

depends essentially only on the propagating part of the sound, i.e., on the reactive property of the system, and the reactive property of nematics is known[8] to be isotropic to the first order. On the other hand, the strength of the acoustic streaming depends on the reactive property as well as the dissipative property of the material; the latter is anisotropic in nematics. Rigorously speaking, to find acoustic streaming, we should solve the acoustic equation of motion in a nematic with at least the anisotropic viscosity included. However, since our primary interest is to explain the basic mechanism of the occurrence of the streaming pattern, we used the following approximations. We first solve the acoustic equation of motion for a sandwiched isotropic fluid film between two solid media by taking into account only the first-order effect of the viscosity since it is small. The anisotropy of the viscosity is accounted for by two viscosity coefficients: a bulk-viscosity coefficient obtained from attenuation of longitudinal sound wave in unoriented nematics and a shear-viscosity coefficient for attenuation of shear wave. The wave vector dependence of both viscosity coefficients for an oriented nematic is neglected. Using the solution of the acoustic modes obtained in this manner, we can then calculate the acoustic streaming induced by beating the various acoustic modes. We are only interested in the time-independent tilt of the director, and hence, we consider only the dc flow reorientation mechanism. Vibration of the director at the ultrasonic frequency is ignored. Therefore, a direct coupling between the sound wave and the director orientation is not considered. The flow-induced anisotropy should of course change the characteristics of the acoustic modes, but the effect is of higher order and can be neglected. We also assume that the shear wave will not affect the molecular alignment at the boudary surfaces. This certainly deserves further investigation and a study of Fredericksz transition with ultrasonic shear wave on the boundary, for instance, could be very interesting. Despite all these approximations; we believe that our theory, described below, does give a proper account of the basic mechanism responsible for the observed sound-induced flow-reorientation pattern.

A. Acoustic waves in a sandwiched fluid film (Ref. 9)

In order to calculate the sound motion in a sandwiched fluid film we use the configuration in Fig. 1. The sound propagation is along $\hat{x}$ and the film normal is along $\hat{z}$ with the solid-fluid interfaces at $z=\pm h$. The y dependence of the problem can be neglected. Acoustic wave propagation in nematic liquid crystals can be described well by treating

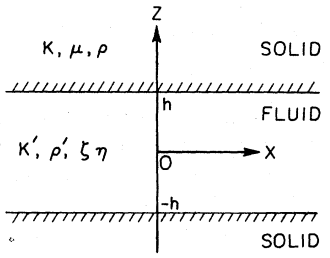

FIG. 1. Geometry of the sandwiched film in our calculations. Upper and lower solids are identical with K being the bulk modulus, μ, the shear modulus; and ρ, the density. The fluid has K' being the bulk modulus, ρ', the density, ζ, the bulk viscosity; and η, the shear viscosity. The sound waves propagate along the x axis.

the liquid-crystalline medium as a simple isotropic fluid.[8] The anisotropy of the dissipation can be taken into account by using "effective" viscosities appropriate to the process under consideration. We neglected here the directional dependence of the viscosity coefficients. We believe the basic propagation structures of acoustic waves will not be affected by this approximation. The solid is isotropic. The material constants of the solid are bulk modulus K, shear modulus μ, and density ρ, and those of the fluid are bulk modulus K' (inverse of compressibility), density ρ', bulk viscosity ζ, and shear viscosity η. Dissipation in the solid can be neglected in the present case.

The equation of motion for the solid is given by[9]

$$\rho\frac{\partial^2\vec{u}}{\partial t^2}=(K+\tfrac{4}{3}\mu)\nabla\nabla\cdot\vec{u}-\mu\nabla\times\nabla\times\vec{u}\,, \tag{1}$$

where $\vec{u}$ is the displacement vector and is related to the mass velocity $\vec{v}$ by $\vec{u}=-\vec{v}/i\omega$ when the motion is sinusoidal. The fluid dynamics is described by the Navier-Stokes equation

$$\rho'\left(\frac{\partial\vec{v}}{\partial t}+(\vec{v}\cdot\nabla)\vec{v}\right)=-\nabla p+(\zeta+\tfrac{4}{3}\eta)\nabla\nabla\cdot\vec{v}-\eta\nabla\times\nabla\times\vec{v}\,, \tag{2}$$

supplemented by the equation of continuity

$$\frac{\partial\rho'}{\partial t}+\nabla\cdot(\rho'\vec{v})=0\,, \tag{3}$$

where p is the pressure. Linearization of Eqs. (2) and (3) leads to

$$\rho'\left(\frac{\partial\vec{v}}{\partial t}\right)=-\nabla p+(\zeta+\tfrac{4}{3}\eta)\nabla\nabla\cdot\vec{v}-\eta\nabla\times\nabla\times\vec{v} \tag{2'}$$

and

$$\frac{\partial\rho'}{\partial t}+\rho'\nabla\cdot\vec{v}=0\,. \tag{3'}$$

Just like any other vector, the mass velocity,

$\vec{v}$, can be split into an irrotational part $\vec{v}_{ir}$ and an incompressible part $\vec{v}_{ic}$, i.e., $\vec{v}=\vec{v}_{ir}+\vec{v}_{ic}$, where $\vec{v}_{ir}=\nabla\Phi$ and $\vec{v}_{ic}=\nabla\times\vec{\Psi}$, Φ and $\vec{\Psi}$ being the scalar and vector potentials, respectively. Since we have neglected the directional dependence of viscosities, the irrotational part and the incompressible part are decoupled from each other in Eqs. (1), (2′), and (3′). Because of the symmetry of the problem, only the y component of $\vec{\Psi}$ is nonvanishing. Using these potentials, the solutions of the equations of motion, Eqs. (1), (2′), and (3′), for sound propagating along $\hat{x}$ in the solid-fluid-solid sandwiched system can be written in the form

$$\left.\begin{aligned}\Phi_1&=\phi_1\exp[-\gamma(z-h)]\\ \Psi_1&=\psi_1\exp[-\beta(z-h)]\end{aligned}\right\}\ \text{for } z>h\,,$$

$$\left.\begin{aligned}\Phi'&=\phi'\exp(i\alpha z)+\phi''\exp(-i\alpha z)\\ \Psi'&=\psi'\exp[i\delta(z-h)]+\psi''\exp[-i\delta(z+h)]\end{aligned}\right\}\quad \text{for } -h\le z\le h\,, \tag{4}$$

$$\left.\begin{aligned}\Phi_2&=\phi_2\exp[\gamma(z+h)]\\ \Psi_2&=\psi_2\exp[\beta(z+h)]\end{aligned}\right\}\ \text{for } z<-h\,,$$

where we have dropped a common propagation factor $\exp[i(kx-\omega t)]$. From Eq. (1) we find

$$k^2-\beta^2=\omega^2/b^2 \text{ and } k^2-\gamma^2=\omega^2/c^2\,, \tag{5}$$

where b and c are, respectively, the transverse and longitudinal sound velocities in the solid given by $b^2=\mu/\rho$ and $c^2=(K+\frac{4}{3}\mu)/\rho$. The real part of β and γ should be positive in order for the sound amplitude to be finite in the solid. Similarly from Eqs. (2′) and (3′) and a constitutive thermodynamic relation $\nabla p=K'\nabla\rho'/\rho'$ we find

$$\delta=-(1+i)\delta_0\,,\quad \delta_0=[\omega\rho'/2\eta(\omega)]^{1/2}\,, \tag{6}$$

and

$$\frac{\omega^2}{\alpha^2+k^2}=a^2-i\epsilon\,,\quad \epsilon=\frac{\omega}{\rho'}\left[\zeta(\omega)+\tfrac{4}{3}\eta(\omega)\right], \tag{7}$$

where $a=(K'/\rho')^{1/2}$ is the bulk sound velocity in the fluid. Note that the viscosities ζ and η depend on the frequency.[10] The amplitudes ϕ's and ψ's are to be determined by boundary conditions.

B. Acoustic modes in the sandwiched film

We now impose the boundary conditions to relate the coefficients ϕ_1, ψ_1, etc., and to determine the eigenmodes. The boundary conditions are that stress and velocity are continuous across the boundaries. At $z=h$, they can be written explicitly (for σ_{zz} continuous)

$$\begin{aligned}-\rho\omega^2\phi_1&+2\rho(\omega^2/k_t^2)(k^2\phi_1-ik\beta\psi_1)\\ &=-(\rho'\omega^2+2i\omega\eta k^2)[\phi'\exp(i\alpha h)+\phi''\exp(-i\alpha h)]\\ &\quad+2i\omega\eta k\,\delta[\psi'-\psi''\exp(-2i\,\delta h)]\,,\end{aligned} \tag{8}$$

(for σ_{zx} continuous)

$$\begin{aligned}&\rho(\omega^2/k_t^2)[(k^2+\beta^2)\psi_1+2ik\gamma\phi_1]\\ &\quad=i\omega\eta\{(-k^2+\delta^2)[\psi'+\psi''\exp(-2i\,\delta h)]\\ &\qquad-2k\alpha[\phi'\exp(i\alpha h)-\phi''\exp(-i\alpha h)]\}\,,\end{aligned} \tag{9}$$

(for v_z continuous)

$$\begin{aligned}-\gamma\phi_1+ik\psi_1&=i\alpha[\phi'\exp(i\alpha h)-\phi''\exp(-i\alpha h)]\\ &\quad+ik[\psi'+\psi''\exp(-2i\,\delta h)]\,,\end{aligned} \tag{10}$$

(for v_x continuous)

$$\begin{aligned}ik\phi_1+\beta\psi_1&=ik[\phi'\exp(i\alpha h)+\phi''\exp(-i\alpha h)]\\ &\quad-i\,\delta[\psi'-\psi''\exp(-2i\,\delta h)]\,,\end{aligned} \tag{11}$$

where $k_t=\omega/b$. With ϕ_1 and ψ_1 replaced by ϕ_2 and ψ_2 and h by $-h$, we find a similar set of equations at $z=-h$. Solution of these eight linearly coupled equations for the eight amplitude coefficients is an eigenvalue problem.

1. Low-viscosity limit

The complete solution of Eqs. (8)–(11) and the complementary equations at $z=-h$ is too complex to be illuminating. We can, however, simplify the calculation by first neglecting the viscosities and later taking them into account as a small perturbation. In the limit that ζ and $\eta\to 0$, the shearing force near the fluid-solid boundary becomes negligibly small; Eq. (11) gives $\psi'=0$, and Eqs. (8)–(10) reduce to

$$\begin{aligned}-\rho\phi_1&+(2\rho/k_t^2)(k^2\phi_1-ik\beta\psi_1)\\ &=-\rho'[\phi'\exp(i\alpha h)+\phi''\exp(-i\alpha h)]\,,\end{aligned} \tag{8′}$$

$$(k^2+\beta^2)\psi_1+2ik\gamma\phi_1=0\,, \tag{9′}$$

$$-\gamma\phi_1+ik\psi_1=i\alpha[\phi'\exp(i\alpha h)-\phi''\exp(-i\alpha h)]\,, \tag{10′}$$

with a similar set of equations at $z=-h$. The condition for these six linearly coupled equations to have nontrivial solutions leads to the characteristic equation[11]

$$\begin{aligned}\frac{\rho}{\rho'}\frac{\alpha}{\gamma}\frac{1}{k_t^4}&[(k^2+\beta^2)^2-4k^2\gamma\beta]\\ &=-\tan(\alpha h)\ \text{(for odd modes)}\,,\\ &=\cot(\alpha h)\ \text{(for even modes)}\,,\end{aligned} \tag{12}$$

from which we can determine the wave vector k, and hence α, β, and γ, in terms of the fluid thick-

ness $2h$. The odd and even modes here refer to the symmetry of the fluid velocity with respect to the $z=0$ plane.

Equation (12) has two types of solutions depending on whether α is real or imaginary. When α is real, the sound waves in the fluid can be described as bulk longitudinal waves bouncing back and forth between the solid plates. They form the waveguide modes. Their amplitude coefficients are

$$\left.\begin{aligned}\phi' &= \phi_A[-i-\cot(\alpha_A h)]\exp(-i\alpha_A h)\\ \phi'' &= \phi_A[i-\cot(\alpha_A h)]\exp(i\alpha_A h)\end{aligned}\right\}$$

(for even modes) (13)

and

$$\left.\begin{aligned}\phi' &= \phi_B[-i+\tan(\alpha_B h)]\exp(-i\alpha_B h)\\ \phi'' &= \phi_B[i+\tan(\alpha_B h)]\exp(i\alpha_B h)\end{aligned}\right\}$$

(for odd modes), (14)

where ϕ_A and ϕ_B are constants. In the following, we use subscripts A and B to describe the even- and odd-waveguide modes, respectively. We shall see that within the range of the film thickness of our interest, there is only one mode of each symmetry. From Eqs. (13) and (14), we find the fluid velocities for the waveguide modes as

$$v_{Ax} = -i\phi_A \frac{2k_A}{\sin(\alpha_A h)}\cos(\alpha_A z)\exp[i(k_A x-\omega t)]\,,$$

$$v_{Az} = \phi_A \frac{2\alpha_A}{\sin(\alpha_A h)}\sin(\alpha_A z)\exp[i(k_A x-\omega t)]\,, \tag{15}$$

and

$$v_{Bx} = i\phi_B \frac{2k_B}{\cos(\alpha_B h)}\sin(\alpha_B z)\exp[i(k_B x-\omega t)]\,,$$

$$v_{Bz} = \phi_B \frac{2\alpha_B}{\cos(\alpha_B h)}\cos(\alpha_B z)\exp[i(k_B x-\omega t)]\,. \tag{16}$$

We also obtain from Eqs. (8′)–(10′),

$$\begin{aligned}\phi_{1j} &= [2\alpha_j(k_j^2+\beta_j^2)/\gamma_j k_t^2]\,\phi_j\,,\\ \psi_{1j} &= -(4ik_j\alpha_j/k_t^2)\phi_j\,,\end{aligned} \tag{17}$$

where $j=A$ or B.

When α is pure imaginary, the modes are the surface-like modes, since for a single solid-fluid interface they correspond to surface waves on the interface with amplitudes decaying exponentially on both sides. There are an even and an odd surface-like modes. The odd mode exists only for $h \gtrsim 226\ \mu$m in the case of nematic p-methoxybenzylidene-p'-butylaniline (MBBA) film between glass plates. In our study, $h<40\mu$m, and only the even surface-like mode is present. We designate it as mode C and write $\bar{\alpha}_C=-i\alpha_C$ which is a real number $(k_C^2-\bar{\alpha}_C^2=\omega^2/a^2)$. The amplitude coefficients are then given by

$$\begin{aligned}\phi' &= \phi_C[-1+\coth(\bar{\alpha}_C h)]\exp(\bar{\alpha}_C h)\,,\\ \phi'' &= \phi_C[1+\coth(\bar{\alpha}_C h)]\exp(-\bar{\alpha}_C h)\,,\end{aligned} \tag{18}$$

and

$$\begin{aligned}\phi_{1C} &= [2\bar{\alpha}_C(k_C^2+\beta_C^2)/\gamma_C k_t^2]\phi_C\,,\\ \psi_{1C} &= -(4ik_C\bar{\alpha}_C/k_t^2)\phi_C\,,\end{aligned} \tag{19}$$

where ϕ_C is a constant. The fluid velocity of this mode is

$$v_{Cx} = i\phi_C \frac{2k_C}{\sinh(\bar{\alpha}_C h)}\cosh(\bar{\alpha}_C z)\exp[i(k_C x-\omega t)]\,,$$

$$v_{Cz} = \phi_C \frac{2\bar{\alpha}_C}{\sinh(\bar{\alpha}_C h)}\sinh(\bar{\alpha}_C z)\exp[i(k_C x-\omega t)]\,. \tag{20}$$

2. *Correction due to viscosity*

The fluid viscosities are low enough so that they can be treated as small perturbations on the above formalism. As shown in Eq. (7), the wave vector k now has a small imaginary part which acts as the attenuation coefficient. Then, from Eq. (5), β and γ also have imaginary parts, which suggests that there is a net power transfer from solid to fluid. As the wave propagates the power in the solid is continuously drawn into the fluid and gets dissipated there.

In the absence of fluid viscosities, the incompressible part of the fluid motion described by ψ' and ψ'' vanishes. Now, this is no longer true. However, with low viscosities, δ_0 in Eq. (6) is very large ($|\delta/k| \gg 1$). From Eq. (11) and a corresponding expression at $z=-h$ we find $|\psi'| \sim |\psi''| \sim |(k/\delta)\phi'|$. It can then be seen that terms involving the irrotational part in Eqs. (8)–(10) are smaller than the other terms by a factor of $|k/\delta|$ and hence have little effect on the eigensolutions obtained earlier. Physically, the viscosities set up a boundary fluid layer of thickness $\sim\delta_0^{-1}$ next to the solid-fluid interface. For large δ_0, the layer is so thin that it can hardly exert force on the solid and hence has little effect on the stress continuity conditions Eqs. (8) and (9). The vertical fluid velocity v_z in the incompressible part is very small and gives very little correction to Eq. (10). Therefore, we can first solve Eqs. (8)–(10) together with similar equations at $z=-h$ by letting $\psi'=\psi''=0$, and then, knowing ϕ', ϕ'', ϕ_1, ϕ_2, ψ_1, and ψ_2, we find ψ' and ψ'' from Eq. (11) and the equivalent one at $z=-h$. We obtain, with $\delta_0 h \gg 1$, for the three

modes A, B, and C,

$$\psi_A' = (1-i)\bar{\psi}_A',$$

$$\bar{\psi}_A' = \frac{k_A}{\delta_0}\left(\cot(\alpha_A h) + \frac{\alpha_A(k_A^2+\beta_A^2-2\beta_A\gamma_A)}{\gamma_A k_t^2}\right)\phi_A, \quad (21)$$

$$\psi_B' = (1-i)\bar{\psi}_B',$$

$$\bar{\psi}_B' = \frac{k_B}{\delta_0}\left(-\tan(\alpha_B h) + \frac{\alpha_B(k_B^2+\beta_B^2-2\beta_B\gamma_B)}{\gamma_B k_t^2}\right)\phi_B, \quad (22)$$

$$\psi_C' = (1-i)\bar{\psi}_C',$$

$$\bar{\psi}_C' = \frac{k_C}{\delta_0}\left(-\coth(\bar{\alpha}_C h) + \frac{\bar{\alpha}_C(k_C^2+\beta_C^2-2\beta_C\gamma_C)}{\gamma_C k_t^2}\right)\phi_C, \quad (23)$$

and a similar set of expressions for ψ''. The incompressible fluid velocity close to $z=h$ is given by

$$v_{jx} = 2i\delta_0\bar{\psi}_j' \exp[(1-i)\delta_0(z-h) + i(k_j x - \omega t)],$$
$$v_{jz} = (1+i)k_j\bar{\psi}_j' \exp[(1-i)\delta_0(z-h) + i(k_j x - \omega t)], \quad (24)$$

where $j = A$, B, or C.

From Eqs. (15), (16), (20), and (24), the total fluid velocities for modes A, B, and C are now given by[12]

$$v_{Ax} = i\left(-\phi_A\frac{2k_A}{\sin(\alpha_A h)}\cos(\alpha_A z) + 2\delta_0\bar{\psi}_A'\{\exp[(1-i)\delta_0(z-h)] + \exp[(i-1)\delta_0(z+h)]\}\right)\exp[i(k_A x - \omega t)],$$
$$v_{Az} = \left(\phi_A\frac{2\alpha_A}{\sin(\alpha_A h)}\sin(\alpha_A z) + (1+i)k_A\bar{\psi}_A'\{\exp[(1-i)\delta_0(z-h)] - \exp[(i-1)\delta_0(z+h)]\}\right)\exp[i(k_A x - \omega t)], \quad (25)$$

$$v_{Bx} = i\left(\phi_B\frac{2k_B}{\cos(\alpha_B h)}\sin(\alpha_B z) + 2\delta_0\bar{\psi}_B'\{\exp[(1-i)\delta_0(z-h)] - \exp[(i-1)\delta_0(z+h)]\}\right)\exp[i(k_B x - \omega t)],$$
$$v_{Bz} = \left(\phi_B\frac{2\alpha_B}{\cos(\alpha_B h)}\cos(\alpha_B z) + (1+i)k_B\bar{\psi}_B'\{\exp[(1-i)\delta_0(z-h)] + \exp[(i-1)\delta_0(z+h)]\}\right)\exp[i(k_B x - \omega t)], \quad (26)$$

and

$$v_{Cx} = i\left(\phi_C\frac{2k_C}{\sinh(\bar{\alpha}_C h)}\cosh(\bar{\alpha}_C z) + 2\delta_0\bar{\psi}_C'\{\exp[(1-i)\delta_0(z-h)] + \exp[(i-1)\delta_0(z+h)]\}\right)\exp[i(k_C x - \omega t)],$$
$$v_{Cz} = \left(\phi_C\frac{2\bar{\alpha}_C}{\sinh(\bar{\alpha}_C h)}\sinh(\bar{\alpha}_C z) + (1+i)k_C\bar{\psi}_C'\{\exp[(1-i)\delta_0(z-h)] - \exp[(i-1)\delta_0(z+h)]\}\right)\exp[i(k_C x - \omega t)]. \quad (27)$$

C. Acoustic power flow

Acoustic power density is given by[13]

$$\vec{P} = -(\vec{v}\cdot\bar{\sigma}^* + \text{c.c.}), \quad (28)$$

where $\vec{v}$ is the particle velocity, $\bar{\sigma}$ is the stress tensor, and * and c.c. indicate complex conjugate. In the absence of dissipation, the net power flow is obviously in the x direction. Therefore, we consider only P_x.

In fluid, since $\sigma_{xx} = \rho' a^2\nabla\cdot\vec{u}$, and $\sigma_{xy} = \sigma_{xz} = 0$, we have

$$P_x = -\rho' a^2(v_x\nabla\cdot\vec{u}^* + \text{c.c.}), \quad (29)$$

where $\vec{u} = -\vec{v}/i\omega$. The power-flow density in the fluid film per unit length in the y direction is given by

$$W_F = \int_{-h}^{h} P_x\,dz. \quad (30)$$

Thus from Eqs. (15), (16), (20), (29), and (30), we find

$$W_{AF} = \frac{4\rho'\omega k_A}{\sin^2(\alpha_A h)}\left(2h + \frac{1}{\alpha_A}\sin(2\alpha_A h)\right)|\phi_A|^2 \quad \text{(for mode A)}, \quad (31)$$

$$W_{BF} = \frac{4\rho'\omega k_B}{\cos^2(\alpha_B h)}\left(2h - \frac{1}{\alpha_B}\sin(2\alpha_B h)\right)|\phi_B|^2 \quad \text{(for mode } B), \quad (32)$$

and

$$W_{CF} = \frac{4\rho'\omega k_C}{\sinh^2(\bar{\alpha}_C h)}\left(2h + \frac{1}{\bar{\alpha}_C}\sinh(2\bar{\alpha}_C h)\right)|\phi_C|^2 \quad \text{(for mode } C). \quad (33)$$

In a similar manner, the power flow density per unit y dimension in the solid is given by

$$W_S = \int_{-\infty}^{-h} P_x\,dz + \int_{h}^{\infty} P_x\,dz = 2\int_{h}^{\infty} P_x\,dz, \quad (34)$$

where P_x is given by Eq. (28) and $\sigma_{xx} = (K + \frac{4}{3}\mu) \times \partial u_x/\partial x + (K - \frac{2}{3}\mu)\partial u_z/\partial z$, $\sigma_{xy} = 0$, and $\sigma_{xz} = \mu(\partial u_x/\partial z + \partial u_z/\partial x)$. We find for each mode

$$W_{jS}=\frac{2}{\omega}\left[\left(\frac{k_j}{\gamma_j}(\rho\omega^2)+4\mu k_j\gamma_j\right)|\phi_{1j}|^2+\frac{k_j}{\beta_j}\mu(k_j^2+3\beta_j^2)|\psi_{1j}|^2\right.$$
$$\left.+\frac{i}{\beta_j+\gamma_j}[\beta_j(\rho\omega^2)+\mu(3k_j^2\gamma_j+2k_j^2\beta_j+\beta_j^2\gamma_j+2\beta_j\gamma_j^2)](\phi_{1j}\psi_{1j}^*-\phi_{1j}^*\psi_{1j})\right], \quad (35)$$

where $j=A$, B, or C. The above expressions are still valid in the presence of small fluid viscosities; the energy associated with the incompressible motion of the fluid is negligible.

The total acoustic power density per unit y width is the sum of Eqs. (31)–(33) and (35) for all modes.

D. Acoustic streaming

A sound wave in an absorbing medium exerts a net force on the medium to conserve momentum. Such a force causes a stationary flow in a fluid, which is known as acoustic streaming.[14] Formally acoustic streaming is a second-order effect governed by Eq. (2). We can express the variables in Eq. (2) in series of ascending orders,

$$\rho'=\rho_0+\rho_1+\rho_2+\cdots,$$
$$p=p_0+p_1+p_2+\cdots, \quad (36)$$
$$\vec{v}=\vec{v}_1+\vec{v}_2+\cdots,$$

where ρ_0 and p_0 are the equilibrium values, $\vec{v}_1$, ρ_1, and $p_1=K'\rho_1/\rho_0$ come from the solution to the linearized equations (2′) and (3′) as given in Sec. II B, and $\vec{v}_2$, ρ_2, and p_2 come from the second-order solution of Eqs. (2) and (3).

From Eq. (2), the second-order equation of motion is

$$-\nabla p_2+[\zeta(0)+\tfrac{4}{3}\eta(0)]\nabla\nabla\cdot\vec{v}_2-\eta(0)\nabla\times\nabla\times\vec{v}_2=\vec{F}, \quad (37)$$

with

$$\vec{F}\equiv\rho_0[(\vec{v}_1\cdot\nabla)\vec{v}_1^*+\vec{v}_1(\nabla\cdot\vec{v}_1^*)+\text{c.c.}], \quad (38)$$

where we have considered (and shall consider in the following calculations) only the time-independent part of $\vec{v}_2$ and p_2 and accordingly the viscosities are evaluated at zero frequency. The equation of continuity (3) in the second order has the form

$$\nabla\cdot\vec{v}_2+(1/\rho_0)\nabla\cdot(\rho_1\vec{v}_1^*+\text{c.c.})=0. \quad (39)$$

In our case, we can show from the expressions of $\vec{v}_1$ and ρ_1 that

$$\nabla\cdot\vec{v}_2\simeq 0, \quad (40)$$

i.e., the streaming is incompressible. Taking curl of both sides of Eq. (37), we get

$$\eta(0)\,\nabla^2(\nabla\times\vec{v}_2)=\nabla\times\vec{F}. \quad (41)$$

The term $\nabla\times\vec{F}$ in Eq. (41) has two parts: one from mixing of different modes and the other from mixing of each mode with itself. The latter produces a uniform streaming along $\hat{x}$. In the Appendix, we show that the uniform streaming is weak and negligible. We calculate here only streaming from mixing of different modes. In the following, we consider mixing of two parts of $\vec{v}_1=\vec{v}_{1ir}+\vec{v}_{1ic}$ separately and sum up the resultant second order velocities $\vec{v}_2$ at the end.

1. *Mixing of* $\vec{v}_{1ir}$ *and* $\vec{v}_{1ir}$

In the presence of dissipation, we have $k_j=k_j'+ik_j''$ and $\alpha_j=\alpha_j'+i\alpha_j''$ ($j=A$, B, or C). When the viscosities are low $k_j''\ll k_j'$, $\alpha_j''\ll\alpha_j'$, and $\epsilon\ll a^2$. Then it can be shown from Eq. (38) that

$$(\nabla\times F)_y=\rho_0\left(v_{1x}v_{1z}^*\frac{2i\epsilon\omega^2}{a^4}+\text{c.c.}\right)$$

and (42)

$$(\nabla\times F)_x=(\nabla\times F)_z=0.$$

Equation (41), with the constraint Eq. (40), can be readily integrated to yield the following particular solutions:

a. Mixing of modes A and B.

$$v_{2x}^{AB}=A_1[C_1\sin(\alpha_A z)\cos(\alpha_B z)+C_2\cos(\alpha_A z)\sin(\alpha_B z)]\exp[i(k_A'-k_B')x]\exp[-(k_A''+k_B'')x]+\text{c.c.},$$
$$v_{2z}^{AB}=A_1[C_3\sin(\alpha_A z)\sin(\alpha_B z)+C_4\cos(\alpha_A z)\cos(\alpha_B z)](-i)\exp[i(k_A'-k_B')x]\exp[-(k_A''+k_B'')x]+\text{c.c.}, \quad (43)$$

where

$$A_1=\frac{-2\phi_A\phi_B^*\rho_0\epsilon}{\sin(\alpha_A h)\cos(\alpha_B h)(k_A-k_B)^2a^2\eta(0)},$$

$$C_1=-\alpha_A\alpha_B(k_A+k_B),\quad C_2=(k_f^2-k_Ak_B)(k_A+k_B),\quad C_3=-\alpha_A(k_f^2-k_Ak_B+\alpha_B^2),\quad C_4=-\alpha_B(k_f^2-k_Ak_B+\alpha_A^2),$$

and

$$k_f = \omega/a\,.$$

b. Mixing of modes B and C

$$\begin{aligned} v_{2x}^{BC} &= A_2[C_5\sin(\alpha_B z)\cosh(\bar{\alpha}_C z) + C_6\cos(\alpha_B z)\sinh(\bar{\alpha}_C z)]\exp[i(k_B' - k_C')x]\exp[-(k_B'' + k_C'')x] + \text{c.c.}\,, \\ v_{2z}^{BC} &= A_2[C_7\sin(\alpha_B z)\sinh(\bar{\alpha}_C z) + C_8\cos(\alpha_B z)\cosh(\bar{\alpha}_C z)](-i)\exp[i(k_B' - k_C')x]\exp[-(k_B'' + k_C'')x] + \text{c.c.}\,, \end{aligned} \tag{44}$$

where

$$A_2 = \frac{-2\phi_B\phi_C^*\rho_0\epsilon}{\cos(\alpha_B h)\sinh(\bar{\alpha}_C h)(k_B - k_C)^2 a^2\eta(0)}\,,$$

$$C_5 = -(k_f^2 - k_B k_C)(k_B + k_C)\,,\quad C_6 = -\alpha_B\bar{\alpha}_C(k_B + k_C)\,,\quad C_7 = \bar{\alpha}_C(\alpha_B^2 + k_f^2 - k_B k_C)\,,\quad C_8 = \alpha_B(\bar{\alpha}_C^2 - k_f^2 + k_B k_C)\,.$$

c. Mixing of modes A and C

$$\begin{aligned} v_{2x}^{AC} &= A_3[C_9\sin(\alpha_A z)\sinh(\bar{\alpha}_C z) + C_{10}\cos(\alpha_A z)\cosh(\bar{\alpha}_C z)]\exp[i(k_A' - k_C')x]\exp[-(k_A'' + k_C'')x] + \text{c.c.}\,, \\ v_{2z}^{AC} &= A_3[C_{11}\sin(\alpha_A z)\cosh(\bar{\alpha}_C z) + C_{12}\cos(\alpha_A z)\sinh(\bar{\alpha}_C z)](-i)\exp[i(k_A' - k_C')x]\exp[-(k_A'' + k_C'')x] + \text{c.c.}\,, \end{aligned} \tag{45}$$

where

$$A_3 = \frac{-2\phi_A\phi_C^*\rho_0\epsilon}{\sin(\alpha_A h)\sinh(\bar{\alpha}_C h)(k_A - k_C)^2 a^2\eta(0)}\,,$$

$$C_9 = -\alpha_A\bar{\alpha}_C(k_A + k_C)\,,\quad C_{10} = (k_f^2 - k_A k_C)(k_A + k_C)\,,\quad C_{11} = \alpha_A(\bar{\alpha}_C^2 - k_f^2 + k_A k_C)\,,\quad C_{12} = -\bar{\alpha}_C(\alpha_A^2 + k_f^2 - k_A k_C)\,.$$

2. Mixing of $\vec{v}_{\text{lic}}$ with $\vec{v}_{\text{lic}}$

Because of the large δ_0, the incompressible part Ψ or $\vec{v}_{1\text{lc}}$ in fluid decays very rapidly away from the solid-fluid interface as seen from Eqs. (4) and (6). Therefore, Eq. (41) can be approximated by[15]

$$\partial F_x/\partial z = \eta(0)\partial^3 v_{2x}/\partial z^3\,. \tag{46}$$

With the expression of $\vec{F}$ in Eq. (38), we find readily the following particular solution for Eq. (46):

$$\begin{aligned} v_{2x}^{ij} &= \frac{\rho_0}{\eta(0)}\bar{\psi}_i'\bar{\psi}_j'^*\{\exp[2\delta_0(z-h)] \pm \exp[-2\delta_0(z+h)]\}[k_i(1+i) + k_j(1-i)]\exp[i(k_i - k_j)x]\exp[-(k_i'' + k_j'')x] + \text{c.c.}, \\ v_{2z}^{ij} &= O(k/\delta_0)\,, \end{aligned} \tag{47}$$

where plus sign applies for $(i,j) = (A,C)$ and minus for $(i,j) = (A,B)$ and (B,C).

3. Mixing of $\vec{v}_{\text{lic}}$ and $\vec{v}_{\text{lir}}$

By the same reason as stated in Sec. II C 2, Eq.(46) applies to the present case. The particular solution is

$$\begin{aligned} v_{2x}^{AB} &= \phi_A\bar{\psi}_B'^*\alpha_A\frac{\sin(\alpha_A z)}{\sin(\alpha_A h)}B_1\exp[i(k_A' - k_B')x - (k_A'' + k_B'')x] \\ &\quad + \phi_B\bar{\psi}_A'^*\alpha_B\frac{\cos(\alpha_B z)}{\cos(\alpha_B h)}B_2\exp[i(k_B' - k_A')x - (k_A'' + k_B'')x] + \text{c.c.}\,, \\ v_{2x}^{BC} &= \phi_B\bar{\psi}_C'^*\alpha_B\frac{\cos(\alpha_B z)}{\cos(\alpha_B h)}B_2\exp[i(k_B' - k_C')x - (k_B'' + k_C'')x] \\ &\quad + \phi_C\bar{\psi}_B'^*\alpha_C\frac{\sinh(\bar{\alpha}_C z)}{\sinh(\bar{\alpha}_C h)}B_1\exp[i(k_C' - k_B')x - (k_B'' + k_C'')x] + \text{c.c.}\,, \\ v_{2x}^{AC} &= \phi_A\bar{\psi}_C'^*\alpha_A\frac{\sin(\alpha_A z)}{\sin(\alpha_A h)}B_2\exp[i(k_A' - k_C')x - (k_A'' + k_C'')x] \\ &\quad + \phi_C\bar{\psi}_A'^*\bar{\alpha}_C\frac{\sinh(\bar{\alpha}_C z)}{\sinh(\bar{\alpha}_C h)}B_2\exp[i(k_C' - k_A')x - (k_A'' + k_C'')x] + \text{c.c.}, \\ v_{2z} &= O(k/\delta_0)\,, \end{aligned} \tag{48}$$

where

$$B_1 = \frac{-(1+i)2\rho_0\{\exp[(1+i)\delta_0(z-h)] + \exp[-(1+i)\delta_0(z+h)]\}}{\eta(0)}$$

and

$$B_2 = \frac{-(1+i)2\rho_0\{\exp[(1+i)\delta_0(z-h)] - \exp[-(1+i)\delta_0(z+h)]\}}{\eta(0)} .$$

4. General solution

The general second-order solution should include the homogeneous solution of Eqs. (40) and (41) in order to satisfy the boundary conditions $\vec{v}_2 = 0$ at $z = \pm h$. In the limit that k/δ_0 and $(k_i - k_j)h$ are small, the homogeneous solutions are[15]

$$\begin{aligned}
v_{2x}^{AB} &= 2D_1(k'_A - k'_B)z \exp[i(k'_A - k'_B)x \\
&\quad - (k''_A + k''_B)x] + \text{c.c.}, \\
v_{2z}^{AB} &= -i[D_2 + D_1(k'_A - k'_B)^2 z^2] \exp[i(k'_A - k'_B)x \\
&\quad - (k''_A + k''_B)x] + \text{c.c.}, \\
v_{2x}^{BC} &= 2D_3(k'_B - k'_C)z \exp[i(k'_B - k'_C)x - (k''_B + k''_C)x] + \text{c.c.}, \\
v_{2z}^{BC} &= -i[D_4 + D_3(k'_B - k'_C)^2 z^2] \exp[i(k'_B - k'_C)x \\
&\quad - (k''_B + k''_C)x] + \text{c.c.}, \qquad (49) \\
\text{and} \\
v_{2x}^{AC} &= [D_5 + 3D_6(k'_A - k'_C)^2 z^2] \exp[i(k'_A - k'_C)x \\
&\quad - (k''_A + k''_C)x] + \text{c.c.}, \\
v_{2z}^{AC} &= -i[D_5(k'_A - k'_C)z + D_6(k'_A - k'_C)^3 z^3] \\
&\quad \times \exp[i(k'_A - k'_C)x - (k''_A + k''_C)x] + \text{c.c.}
\end{aligned}$$

The (complex) constants $D_1 \sim D_6$ are determined from the boundary conditions and the relative phases of the modes. They become real quantities if we replace $(k'_i - k'_j)x$ $(i, j = A, B, \text{ or } C)$ in Eq. (49) by $(k'_i - k'_j)x + \phi_{ij}$ where ϕ_{ij} is the relative phase of the i and j modes.

The complete second-order velocity is then given by the sum of Eqs. (43), (44), (45), (47), (48), and (49).

E. Flow reorientation

Knowing the stationary fluid velocity, we can calculate the associated shear-flow reorientation of the nematic molecules. We assume that initially the molecules are homeotropically aligned. If the induced tilt angle θ of the director from the z axis is small, the equation describing the balance of torques is[1]

$$K_{33}\partial^2\theta/\partial z^2 + \alpha_2 \partial v_{2x}/\partial z = 0 , \qquad (50)$$

where K_{33} is Frank's bend elastic constant[16] and α_2 is Leslie's shear-torque coefficient.[17] We have neglected other shearing terms, $\partial v_{2z}/\partial x$, etc., not only because they are small but also because the pertinent shear-torque coefficient α_3 is small[18] ($|\alpha_3/\alpha_2| \sim 10^{-2}$). Equation (50) is readily integrated to yield, assuming $\theta = 0$ and $d\theta/dz = 0$ at the solid-fluid interface,

$$\theta(x, z) = -\frac{\alpha_2}{K_{33}} \int_z^h v_{2x}(x, z')\, dz' \qquad (51)$$

satisfying the boundary condition that $\theta(x, \pm h) = 0$. Note that although the shear rate in the boundary layer is very large, its direct effect on reorientation is small because

$$\int_{\text{boundary layer}} v_{2x}\, dz'$$

is very small for a thin layer. The effect of the boundary layer comes in indirectly through the boundary conditions leading to large D_i $(i = 1-6)$.

As a result of flow orientation, the optical axis of the nematic substance is now tilted at an angle $\theta(x, z)$ away from $\hat{z}$ in the x-z plane. If the film is placed between crossed polaroids with their axes at 45° with respect to $\hat{x}$ and $\hat{y}$, the optical transmission coefficient of the assembly is given by[19]

$$\begin{aligned}
I/I_0 &= \sin^2[\tfrac{1}{2}\Delta(x)], \\
\Delta(x) &= \frac{2\pi}{\lambda}(n_\parallel - n_\perp)\int_{-h}^{h} \sin^2\theta(x, z)\, dz ,
\end{aligned} \qquad (52)$$

where I and I_0 are, respectively, the transmitted and incident light intensities, λ is the optical wavelength, and $n_\parallel$ and $n_\perp$ are refractive indices of light polarized parallel and perpendicular to the optical axis of the nematic film, respectively.

In order to illustrate the theory, we show the result of numerical calculations of $\vec{v}_2(x, z)$ and $\theta(x, z)$ in Fig. 2. (The parameters used are the same as those for Fig. 7. Note that the vertical axis and accordingly v_{2z} are expanded four times. The angle θ is also exaggerated by four times.) The vortical fluid flow and the associated tilt of the directors are clearly visualized.

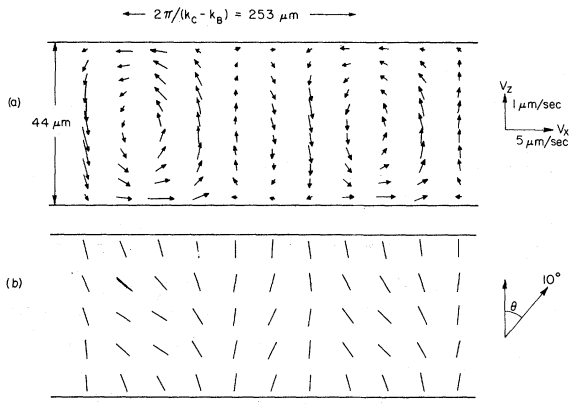

FIG. 2. (a) Fluid flow velocity, and (b) director orientation, calculated from Eqs. (43)–(45), (47)–(49), and (51) for the first three flow vortices along $\hat{x}$ with the same parameters used in the calculation of Fig. 7(b). Both the $\hat{z}$ scales and the tilt angle are expanded four times for illustration.

III. EXPERIMENTAL TECHNIQUE

The experimental setup[6] is shown in Fig. 3. An interdigital surface-wave transducer of fundamental frequency of 12.3 MHz was deposited on a Y-cut X-oriented quartz plate. A surface wave generated on the quartz plate by the transducer was transferred onto one of the glass plates holding a nematic film through a water coupler, and then propagated into the sample region. The sample thickness was controlled by Al or Mylar spacers of various thicknesses to ±2 μm. The inner surfaces of the glass plates were treated by silane surfactants to obtain homeotropic or homogeneous monodomain samples. All experiments reported here were done on MBBA at room temperature. The effects have, however, been seen in other nematics. The observation of the sample was carried out by a polarizing microscope.

The phase velocities and amplitudes of the acoustic modes in the sandwiched medium were measured by the optical diffraction technique.[20] The experimental setup is shown schematically in Fig. 4. A 1.5-mW He–Ne laser beam was directed onto

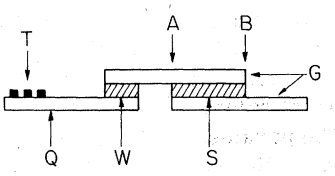

FIG. 3. Sample arrangement. T is the interdigital surface wave transducer, Q is the quartz crystal plate, W is the water film coupler, S is the liquid crystal film, and G is the glass plates.

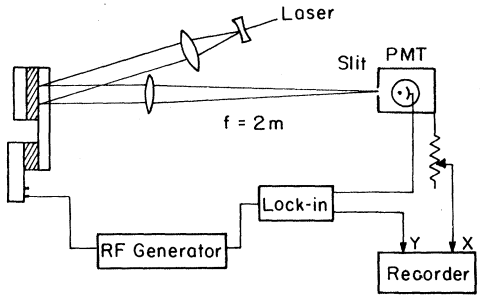

FIG. 4. Block diagram of the optical-diffraction experiment.

the sample and the backward diffracted light was analyzed. The inner surface of one glass plate was partly coated with a thin (~500-Å) Al film to enhance the reflection.

The laser beam was then diffracted by corrugation of the Al film caused by the propagating sound in the film. The diffraction pattern was measured at the focal plane with a photomultiplier behind a slit. For each acoustic mode, the separations of the diffraction peaks should be proportional to k's from which α's can be calculated. The results were calibrated against the free Rayleigh-wave velocity on quartz. The peak height should be proportional to the square of the acoustic amplitude $|v_z|^2$ in the z direction at $z = h$. Using Eqs. (25)–(27) we calculated relative magnitudes of $|\phi_A|$, $|\phi_B|$, and $|\phi_C|$. The absolute *amplitudes* were then determined[21] by measuring the intensity ratio of the first-order diffraction peak to the zeroth-order peak for the strongest mode. Because of the nature of our experiment, the phases of ϕ's could not be obtained. From Eqs. (31), (32), (33), and (35) the absolute acoustic power density per unit width of each mode was obtained. The transducer-sample assembly was mounted on a rail and positioned by a micrometer. The attenuation of each mode was measured by observing the change of the diffraction peak height as the laser-beam probes different regions of the sample along the direction of sound propagation.

IV. RESULTS AND DISCUSSION

We first show in Fig. 5 the results of our diffraction measurements on the phase velocities of the waveguide and surface-like modes in sandwiched nematic films as functions of film thickness. They are compared with the theoretical curves calculated from Eq. (12). The material constants used in the calculation were measured separately as $a = 1.55$ km/sec, $b = 3.38$ km/sec, $c = 5.69$ km/sec, $\rho = 2.45$ g/cm^3, and $\rho' = 1.0$ g/cm^3. There is no adjustable parameter in the calculation. The agree-

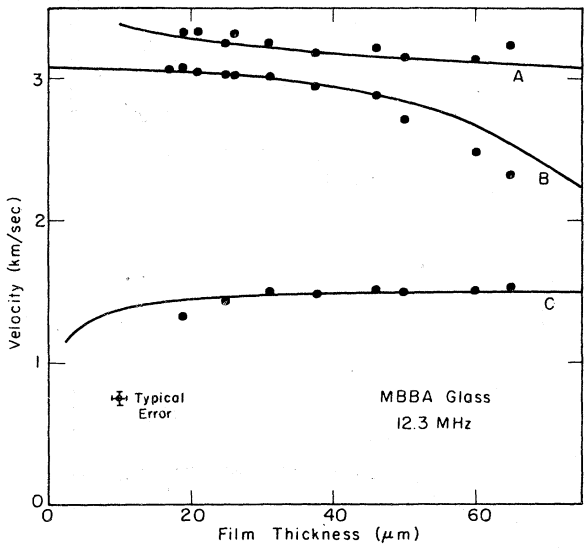

FIG. 5. Phase velocities of modes A, B, and C as functions of film thickness. Dots are experimental data from diffraction measurements and solid curves are calculated from Eq. (12).

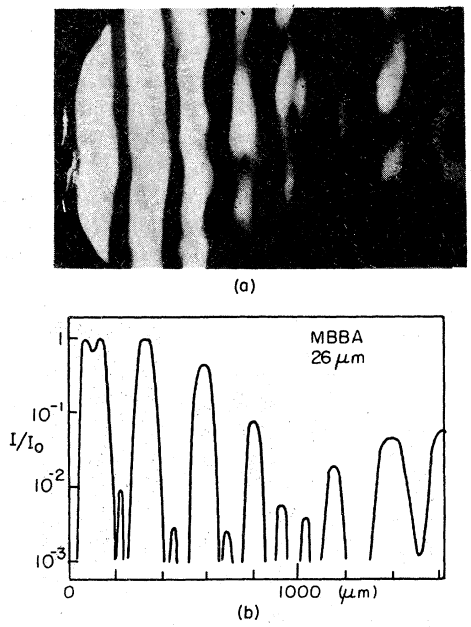

FIG. 6. (a) Photograph of the domain pattern induced by acoustic streaming in a homeotropic MBBA film of 26 μm thick. Sound propagated from left to right. The sample was between crossed polaroids with their axes at 45° with respect to the stripes. Total acoustic power density was about 19 mW/cm. The picture was overexposed to exhibit weaker stripes. (b) Calculated transmission coefficient I/I_0 as a function of x from Eq. (52). The following parameters were used in the calculation: $k_A = 239\ \text{cm}^{-1}$, $k_B = 255\ \text{cm}^{-1}$, $k_C = 526\ \text{cm}^{-1}$, $\phi_A/\phi_B = 0.17$, $\phi_C/\phi_B = 0.1$ and total acoustic power density = 21 mW/cm, aside from the other parameters given in the text.

ment between theory and experiment is good. The small systematic deviation seems to stem from neglecting the viscous stress of the boundary layer, especially σ_{zx} [see Eq. (9)]. In the case of water films,[20] whose viscosity is an order of magnitude smaller than MBBA, the agreement was better.

When a homeotropic nematic film in the presence of acoustic excitation was examined under a microscope between crossed polaroids, a stripe pattern was observed. Typical patterns at the feeding edge (A in Fig. 3) are shown in Figs. 6(a) and 7(a). The acoustic waves propagated from left to right, perpendicular to the stripes. The constrast of the stripes was best when the polaroid axes were at 45° with respect to the stripes. Without acoustic excitation the view was dark. A similar pattern was observed when the polaroids were parallel with the polarizing axes along $\hat{x}$ and the image plane was defocused slightly above or below the sample. This was apparently due to the well-known "lens effect"[22] in the acoustically perturbed nematic film. With increasing acoustic power, the stripe pattern first showed up and then became increasingly clear. However, there was no definite acoustic threshold power for the appearance of the pattern. We simultaneously observed dust particles in the sample undergoing flattened vortex motion around the bright stripes in directions consistent with the flow pattern shown in Fig. 2(a). Judg-

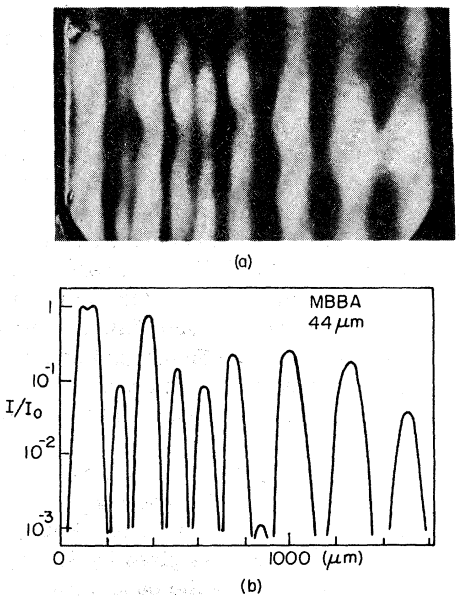

FIG. 7. (a) Same as Fig. 6(a) for a 44-μm-thick film at a total acoustic power density of about 4 mW/cm. (b) Calculated transmission coefficient I/I_0 using the parameters $k_A = 239\ \text{cm}^{-1}$, $k_B = 266\ \text{cm}^{-1}$, $k_C = 515\ \text{cm}^{-1}$, $\phi_A/\phi_B = 0.48$, $\phi_C/\phi_B = 0.33$, and total acoustic power density = 5 mW/cm.

ing from the dust particle trajectories, the size of the vortices in the direction normal to the film was about 10–20 μm in a 30-μm-thick sample. The semiperiodicity of the stripe pattern was independent of the acoustic power. Nor was there any dependence of the pattern on the length of the sample (1–5 cm). In the long samples, the sound wave was completely attenuated at the end so that there was no reflection from the end and hence the stripe pattern cannot be due to standing wave. All these observations can be explained successfully by our theory of flow reorientation due to acoustic streaming (Sec. II).

For a given film thickness, we can calculate the spatial variation of the optical transmission coefficient of the sample between crossed polaroids using Eq. (52) and compare with the stripe pattern observed under microscope. In the calculations, we used values of k's and $|\phi|$'s obtained directly from optical diffraction measurements. We found $\epsilon/a^2 = 7.5\times10^{-3}$ from the measured bulk sound attenuation constant[23] and $\delta_0 = 1.2\times10^4$ cm^{-1} from the shear-wave reflection experiment[24] which gave $\eta(\omega) = 0.27$ P. The constants α's and δ were then calculated from Eqs. (6) and (7). Other parameters used in the calculation were $\eta(0) = 1.0$ P (deduced from capillary viscometer measurement[25]), $\alpha_2 = -0.8$ P,[18] $n_\parallel - n_\perp = 0.2$ [26] at $\lambda = 0.6$ μm, and $K_{33} = 0.7\times10^{-6}$ dyn.[27] Since the relative phases of ϕ's were unknown, they were used as adjustable parameters to fit the observed pattern. Among the measured quantities the absolute amplitudes of the acoustic modes were by far the least accurate because of the instability of the water coupler (W in Fig. 3). They were only reproducible to within 50%, while the relative amplitudes remained unchanged. Therefore, in the calculation, we also adjusted the absolute amplitudes within our experimental accuracy to obtain the best fit. Two examples of the calculated transmission patterns are shown in Figs. 6(b) and 7(b) corresponding to the experimental conditions which led to the observed patterns in Figs. 6(a) and 7(a), respectively. The agreement between theory and experiment is very good. The maximum tilt angle of the director in these cases was 15°–20° and hence Eq. (50) was valid.

For a thin sample such as in the cases of Figs. 6 and 7, mode B is dominant. Since $(k_C - k_B) \gg (k_B - k_A)$ in a thin sample, the stripe domain period at the feeding edge was given by $2\pi/(k_C - k_B)$. In Fig. 8 we compare the observed periodicity (bars) with $2\pi/(k_C - k_B)$ (open circles) calculated from the data of the diffraction measurement shown in Fig. 5. The agreement is very good.

At low-power levels, the transmission coefficient is proportional to the eighth power of the sound amplitude or the applied voltage on the surface wave transducer since from Eqs. (51) and (52), we find $I/I_0 \sim \Delta^2 \sim \theta^4 \sim |v_2|^4 \sim |v_1|^8$. Thus, the pattern showed up suddenly with increase of acoustic power but there was no definite threshold. As the acoustic power was increased further, colored

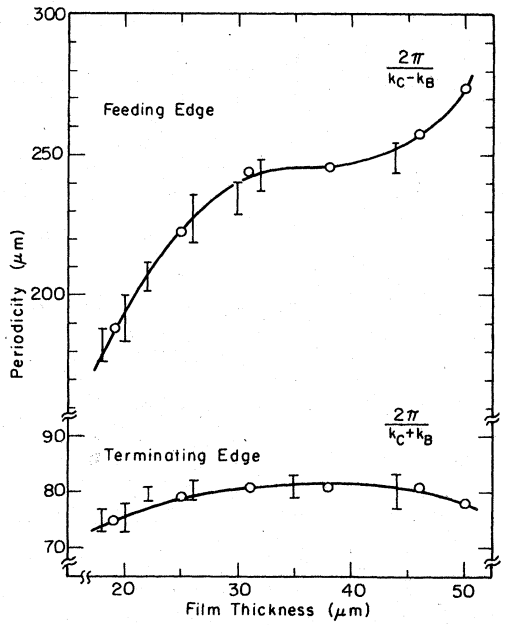

FIG. 8. Comparison of observed periodicities (bars) of stripe domain patterns with calculated values (open circles) of $2\pi/(k_C - k_B)$ at the feeding edge and of $2\pi/(k_B + k_C)$ at the terminating edge. k_B and k_C were obtained from Fig. 5. Curves are guides to the eye.

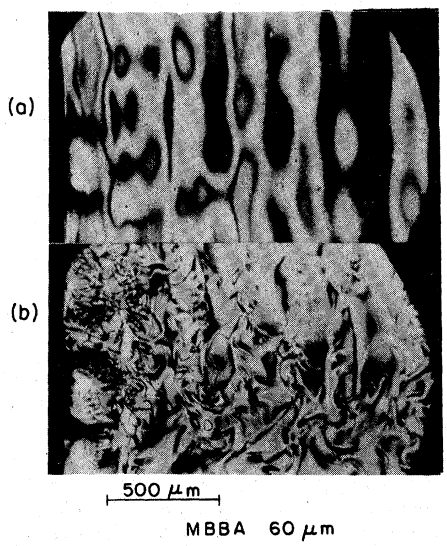

FIG. 9. Patterns observed in an MBBA film under high-acoustic excitation. (a) Showing colored striation (isochromate). (b) Showing dynamic scattering mode.

striations (isochromate) began to appear within each stripe [Fig. 9(a)], and then the molecules could not sustain the homeotropic alignment so that disclinations (apparently 90° walls) grew from the feeding edge. At yet higher-power level, the director orientation was completely randomized, and the disclination lines tumbled around in a way resembling the dynamic scattering mode [Fig. 9(b)]. In the entire process, there was no apparent discontinuous change. The ratio of the power at which the peak intensity of the first stripe reaches a maximum to that of the dynamic scattering mode was about 1 to 3 for all film thicknesses.

A pattern of much shorter periodicity was found at the terminating edge (B in Fig. 3) of the sample as shown in Fig. 10(a). In this case, the film was 26 μm thick and about 1.5 cm long. It was found that towards the end the periodicity was equal to $2\pi/(k_B+k_C)$. Diffraction measurement showed that both mode A and mode C were rather weak in comparison with mode B, and that the forward propagating mode C was almost completely attenuated towards the middle of the sample. Mode B, however, remained strong and propagated to the end of the film. There, the wave was partially transmitted as free Rayleigh wave on glass, partially reflected as mode B, and partially reflected as modes A and C. Mixing of various forward and backward propagating modes again produced acoustic streaming which led to the observed stripe domain pattern. The shortest domain period was given by $2\pi/(k_B+k_C)$, resulting from mixing of the forward propagating mode B with the backward propagating mode C. That the pattern was not produced by reflected waves from the glass edge was ascertained by the fact that the pattern remained unchanged when the glass plates were extended far beyond the nematic film. The pattern was also seen near trapped air bubbles for the same reason. When the sample was long ($\gtrsim$5 cm), all modes were extinguished by attenuation towards the end of the film and hence no pattern was observed at the end of the film. We show in Fig. 8 the observed periodicities at the terminating edge in comparison with the calculated values of $2\pi/(k_B+k_C)$ for different film thicknesses.

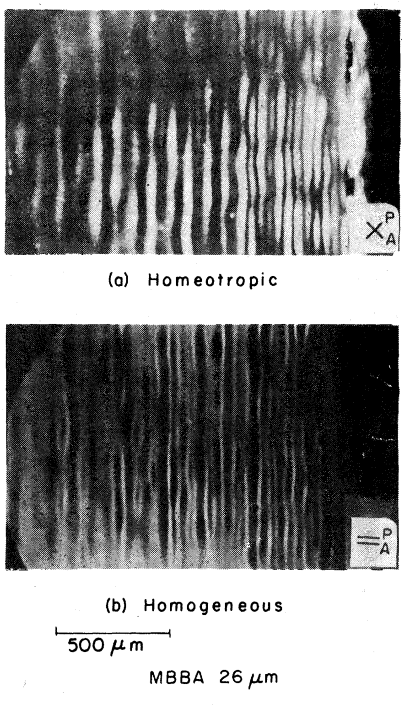

FIG. 10. Domain patterns induced by acoustic streaming at the terminating edge of a 26-μm thick MBBA film. (a) With a homeotropic alignment observed between crossed polaroids. (b) With a homogeneous alignment along the wave propagation direction $\hat{x}$ observed between parallel polaroids with the polarizing axis along $\hat{x}$. The end of the film is on the right.

We found similar effects in homogeneous samples where the molecular alignment was initially along $\hat{x}$. In this case, the semiperiodic pattern was most easily observed with parallel polarizers. The light polarization was along $\hat{x}$ and the pattern was created by the lens effect.[22] This lens effect was again due to molecular reorientation induced by the acoustic streaming and therefore the resultant domain pattern with its semiperiodicity was essentially the same as that in the homeotropic case. In particular, the periodicities of the pattern at the feeding edge and at the terminating end of the film are the same as those in the homeotropic case. As an example, we show in Fig. 10(b) the observed pattern in the homogeneous case at the end of a 26-μm-thick sample. Higher acoustic power was needed to create the pattern in the homogeneous case because the shear term responsible for inducing molecular orientation was now $\partial v_z/\partial x$. This was weak compared to $\partial v_x/\partial z$ which was dominant but had little effect on the molecular orientation in the homogeneous geometry.[28]

It was previously suggested by Kapustina and Statnikov[5] that the semiperiodic pattern could be caused by oscillating directors in the nematic boundary layer driven by the propagating surface acoustic wave through viscoelasticity. Such an explanation has many difficulties.[6] In our experiment, besides the above-mentioned observations related to flow alignment of molecules, we found further direct evidence against this explanation. When we defocused the microscope above and below the film we observed, with convergent illumination, neighboring stripes shifted in opposite directions as shown in Fig. 11. This can only be explained by stationary molecular orientation in the

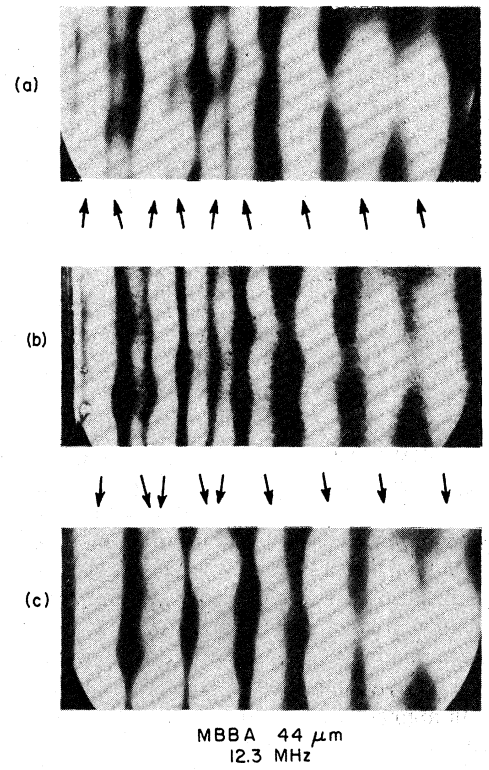

FIG. 11. Domain patterns observed in a 44-μm-thick MBBA film when the microscope was (a) defocused up from the middle of the sample by 200 μm, (b) in focus, and (c) defocused below the middle of the sample by 200 μm.

bulk of the nematic film. The explanation is sketched in Fig. 12. As in Fig. 2, the tilt of the molecules varied semiperiodically along x under acoustic excitation. The optical rays from the left passing through the regions with molecules tilted to the left saw more birefringence and experienced more rotation of polarization. Those passing through the regions with molecules tilted to the right experienced less rotation of polarization. The converse was true for optical rays coming from the right. As a result, Fig. 12 shows that two neighboring stripes in a semiperiodic domain pattern were actually obtained from optical rays coming from opposite directions. Therefore, defocusing above or below the center of the film moved two neighboring stripes either farther apart or closer together. This effect disappeared when parallel illuminating beam was used. We further noted that the turn-off time of the domain pattern was longer for thicker samples (~1 sec for a 60-μm film). This cannot be understood by the model assuming only molecular reorientation in the boundary layer,[5] but can be easily understood as due to slow healing of the deformed director as in the case of William's domains.[29] The acoustic intensity needed to produce the domain pattern decreased rapidly with increase of sample thickness. This is also contradictory to the model of Ref. 5 where it would predict no such acoustic power dependence as long as the sample thickness is larger than the penetration depth δ_0^{-1}.

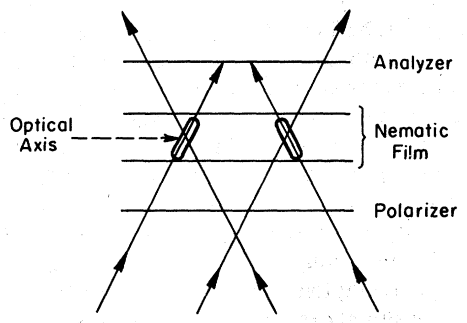

FIG. 12. Schematic drawing to explain the effect shown in Fig. 11. See the text.

From the calculations in Sec. II, it is clear that acoustic streaming of this type is not unique to liquid crystals. We have in fact observed almost identical flow patterns of suspended particles in water films. The fluid motion in water turned out to be more vigorous than that in MBBA at the same acoustic power. This is because the driving force for acoustic streaming is mainly governed by $\eta(\omega)$, which in MBBA is much lower than the viscosity for the steady flow $\eta(0)$ but in water is nearly the same as $\eta(0)$.

We have also examined homeotropic films of a smectic-A liquid crystal CBOOA (p-cyanobenzylidene-p-n-octyloxyaniline). The steady driving force $\vec{F}$ [Eq. (38)] should also appear in a sandwiched smectic film when subjected to surface wave excitation. Due to the smectic layered structure, however, it is extremely difficult to create fluid flow in the material. Moreover, tilting of molecules with respect to the layer normal would be energetically very unfavorable. Accordingly, we could not observe any induced birefringence in the smectic film with high acoustic excitations up to the point where disclination lines started to appear.

V. CONCLUSIONS

A surface Rayleigh wave propagating into a sandwiched nematic film can in general excite several propagating acoustic modes in the film. Nonlinear mixing of these modes in the film produces a steady fluid flow known as acoustic streaming. Because wave vectors of different modes are different, the resultant acoustic streaming is in the form of vortices with semiperiodic spatial variation along the direction of wave propagation. The

fluid flow leads to flow alignment of molecules in the nematic film. Therefore, in the case where original molecular alignment is uniform, the vortical acoustic streaming produces a semiperiodic reorientation of the directors in the nematic film and hence a semiperiodic birefringence pattern. Then when observed with a proper polarizer-analyzer combination, one finds a semiperiodic stripe domain pattern. We have formulated the theory and shown that the theory can indeed explain quantitatively the experimental observation.

We believe the theory can also be used to explain the results of other shear wave experiments, such as the one reported in Ref. 4. In these experiments, there should be no definite threshold acoustic power for any observed phenomenon resulting from acoustic streaming. However, at low power level the visibility of the phenomenon may increase rather suddenly with increase of the acoustic power since the small induced birefringence is proportional to the fourth power of the acoustic amplitudes.

The situation may be completely different in the case[1,2] where homogeneous bulk sound wave propagates along the normal of a homeotropic nematic film. In Helfrich's model, anisotropic interaction of sound wave with the oriented molecules is essential to cause the molecular reorientation and a fluid flow; the intensity of the sound wave is assumed to be uniform throughout the sample.

ACKNOWLEDGMENTS

This work was partially supported by the U.S. Energy Research and Development Administration. One of us (Y.R.S.) is indebted to the Miller Institute of the University of California for partial support.

APPENDIX

We calculate here the uniform streaming caused by mixing of a mode with itself. We use Eqs. (25)–(27) and (38) to find the driving force $\vec{F}$ for the uniform streaming and then the streaming velocity $\vec{v}_2$. The homogeneous solution for $\vec{v}_2$ in this case is of the form $v_{2x} = D_7 + D_8 z^2$ and $y_{2y} = v_{2z} = 0$. Knowing $\vec{v}_2$, we can obtain the tilt angle θ from Eq. (51). As an example, we have calculated the tilt angle $\theta(x,z)$ induced by a uniform streaming in a 44-μm-thick film at 5-mW/cm acoustic power. The maximum value is 2° at $z = \pm 12$ μm. This is negligible in comparison with the maximum tilt angle of ~15° induced by the nonuniform streaming calculated in Sec. II. Physically, one may argue that the uniform streaming which is symmetric in z and has four nodes along z is energetically more difficult to drive than the nonuniform vortical streaming which is asymmetric in z [see Fig. 2(a)] and has three nodes along z.

---

*Research supported by the NSF Grant No. DMR-74-07361.

†Present address: Argonne National Lab., Argonne, Ill. 60439.

[1]W. Helfrich, Phys. Rev. Lett. 29, 1583 (1972). A more transparent treatment was given later by S. Nagai and K. Iizuka, Jpn. J. Appl. Phys. 13, 189 (1974).

[2]L. W. Kessler and S. P. Sawyer, Appl. Phys. Lett. 17, 440 (1970); H. Mailer, K. L. Likins, T. R. Taylor, and J. L. Fergason, *ibid.* 18, 105 (1971); and M. Bertolotti, S. Martellucci, F. Scudieri, and D. Sette, *ibid.* 21, 74 (1972).

[3]L. E. Davis and J. Chambers, Electron. Lett. 7, 287 (1971); and O. A. Kapustina and A. A. Talashev, Sov. Phys. Acoust. 19, 397 (1974).

[4]Y. Kagawa, T. Hatakeyama, and Y. Tanaka, J. Sound Vib. 41, 1 (1975).

[5]O. A. Kapustina and Yu. G. Statnikov, Sov. Phys. JETP 37, 117 (1973); and Sov. Phys. Acoust. 20, 154 (1974).

[6]K. Miyano and Y. R. Shen, Appl. Phys. Lett. 28, 473 (1976).

[7]General review of this phenomenon is found in many references, e.g., M. J. Stephen and J. P. Straley, Rev. Mod. Phys. 46, 617 (1974); and P. G. deGennes, *The Physics of Liquid Crystals* (Oxford, London, 1974).

[8]M. E. Mullen, B. Lüthi, and M. J. Stephen, Phys. Rev. Lett. 28, 799 (1972).

[9]See, for example, L. M. Brekhovskikh, *Waves in Layered Media* (Academic, New York, 1964).

[10]K. Miyano and J. B. Ketterson, Phys. Rev. A 12, 615 (1975).

[11]This equation is identical to Eqs. (1) and (2) of W. C. Wang, P. Staecker, and R. C. M. Li, Appl. Phys. Lett. 16, 291 (1970).

[12]In Ref. 6 only part of this expression was shown. Also note the change in the expressions for the constants ϕ_A, ϕ_B, and ϕ_C.

[13]We use the convention that the actual particle velocity is given by $\vec{v}+\vec{v}^*$.

[14]For a review of acoustic streaming see, for example, W. L. M. Nyborg, in *Physical Acoustics*, edited by W. P. Mason (Academic, New York, 1965), Vol. II-B.

[15]See, for example, Ref. 14, pp. 290–292.

[16]F. C. Frank, Disc. Faraday Soc. 25, 19 (1958).

[17]F. M. Leslie, Quart. J. Mech. Appl. Math. 19, 357 (1966).

[18]Ch. Gähwiller, Phys. Lett. 36A, 31 (1971).

[19]See, for example, M. Born and E. Wolf, *Principles of Optics* (Pergamon, London, 1970), Chap. XIV.

[20]K. Miyano and Y. R. Shen, Appl. Phys. Lett. 28, 699 (1976), and references therein.

[21]G. Cambon, M. Rouzeyre, and G. Simon, Appl. Phys. Lett. 18, 295 (1971). In Ref. 6 the acoustic power was overestimated.

[22]P. A. Penz, Phys. Rev. Lett. 24, 1405 (1970).
[23]D. Eden, C. W. Garland, and R. C. Williamson, J. Chem. Phys. 58, 1861 (1973). The attenuation was reported at 9 and 15 MHz. We obtained the value at 12.3 MHz by interpolation.
[24]P. Martinoty and S. Candau, Mol. Cryst. Liq. Cryst. 14, 243 (1971). It was argued in this reference that the viscosity coefficient η_a (= 0.27 P) should also apply to the shear-wave geometry in our case.
[25]See Ref. 18; $\eta(0) = \eta_1$ in this reference.
[26]M. Brunet-Germain, C. R. Acad. Sci. (Paris) B 271, 1075 (1970).
[27]I. Haller, J. Chem. Phys. 57, 1400 (1972).
[28]J. Fisher and J. Wahl, Opt. Commun. 5, 341 (1972).
[29]M. F. Schiekel and K. Fahrenschon, Appl. Phys. Lett. 19, 391 (1971).

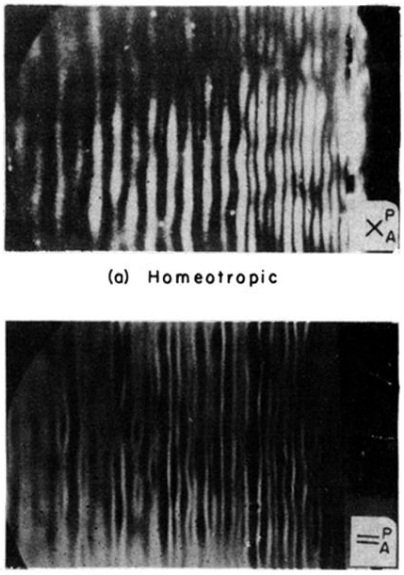

FIG. 10. Domain patterns induced by acoustic streaming at the terminating edge of a 26-μm thick MBBA film. (a) With a homeotropic alignment observed between crossed polaroids. (b) With a homogeneous alignment along the wave propagation direction $\hat{x}$ observed between parallel polaroids with the polarizing axis along $\hat{x}$. The end of the film is on the right.

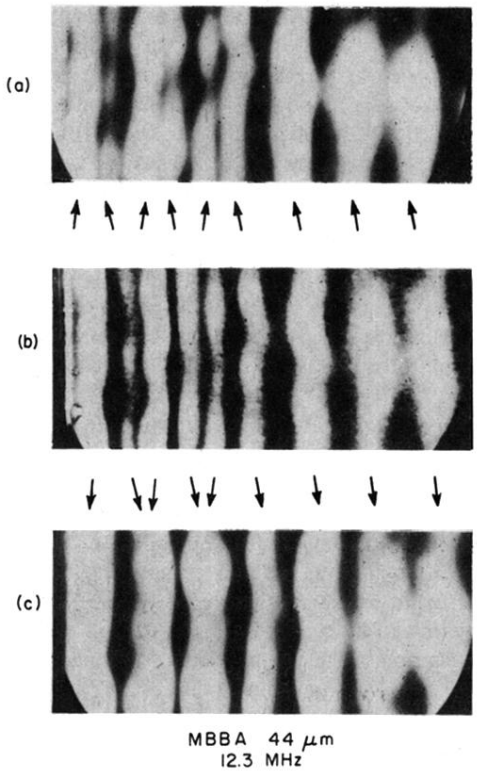

FIG. 11. Domain patterns observed in a 44-μm-thick MBBA film when the microscope was (a) defocused up from the middle of the sample by 200 μm, (b) in focus, and (c) defocused below the middle of the sample by 200 μm.

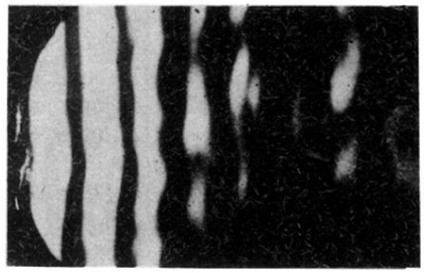

(a)

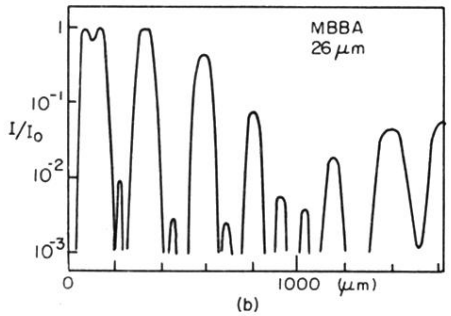

(b)

FIG. 6. (a) Photograph of the domain pattern induced by acoustic streaming in a homeotropic MBBA film of 26 μm thick. Sound propagated from left to right. The sample was between crossed polaroids with their axes at 45° with respect to the stripes. Total acoustic power density was about 19 mW/cm. The picture was over-exposed to exhibit weaker stripes. (b) Calculated transmission coefficient I/I_0 as a function of x from Eq. (52). The following parameters were used in the calculation: $k_A = 239\ \text{cm}^{-1}$, $k_B = 255\ \text{cm}^{-1}$, $k_C = 526\ \text{cm}^{-1}$, $\phi_A/\phi_B = 0.17$, $\phi_c/\phi_B = 0.1$ and total acoustic power density = 21 mW/cm, aside from the other parameters given in the text.

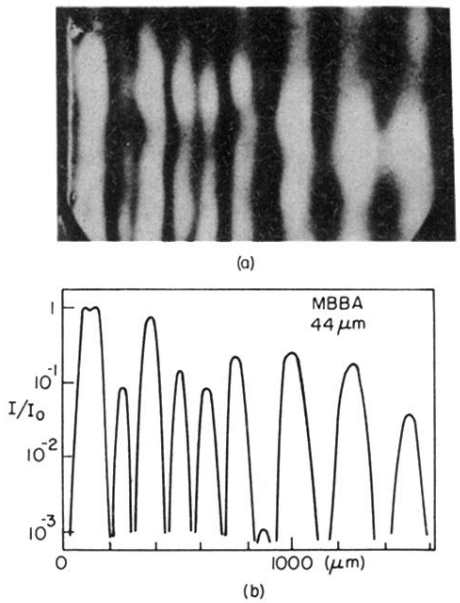

FIG. 7. (a) Same as Fig. 6(a) for a 44-μm-thick film at a total acoustic power density of about 4 mW/cm. (b) Calculated transmission coefficient I/I_0 using the parameters $k_A = 239\ \text{cm}^{-1}$, $k_B = 266\ \text{cm}^{-1}$, $k_C = 515\ \text{cm}^{-1}$, $\phi_A/\phi_B = 0.48$, $\phi_C/\phi_B = 0.33$, and total acoustic power density = 5 mW/cm.

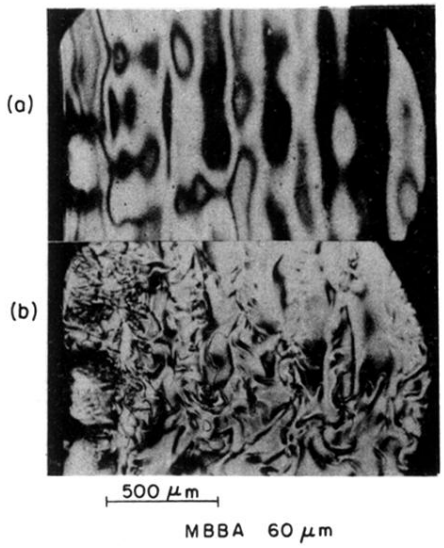

FIG. 9. Patterns observed in an MBBA film under high-acoustic excitation. (a) Showing colored striation (isochromate). (b) Showing dynamic scattering mode.